Draft version March 3, 2014
Preprint typeset using LaTeX style emulateapj v. 5/2/11

arXiv:1402.7129v1 [astro-ph.SR] 28 Feb 2014

PTF1 J191905.19+481506.2 — A PARTIALLY ECLIPSING AM CVN SYSTEM DISCOVERED IN THE PALOMAR TRANSIENT FACTORY

David Levitan[1], Thomas Kupfer[2], Paul J. Groot[1,2], Bruce Margon[3], Thomas A. Prince[1], Shrinivas R. Kulkarni[1], Gregg Hallinan[1], Leon K. Harding[1], Gillian Kyne[4], Russ Laher[5], Eran O. Ofek[6], René G. M. Rutten[7], Branimir Sesar[1], and Jason Surace[5]

Draft version March 3, 2014

ABSTRACT

We report on PTF1 J191905.19+481506.2, a newly discovered, partially eclipsing, outbursting AM CVn system found in the Palomar Transient Factory synoptic survey. This is only the second known eclipsing AM CVn system. We use high-speed photometric observations and phase-resolved spectroscopy to establish an orbital period of 22.4559(3) min. We also present a long-term light curve and report on the normal and super-outbursts regularly seen in this system, including a super-outburst recurrence time of 36.8(4) d. We use the presence of the eclipse to place upper and lower limits on the inclination of the system and discuss the number of known eclipsing AM CVn systems versus what would be expected.

Subject headings: accretion, accretion disks — binaries: close — novae, cataclysmic variables — stars: individual: (PTF1 J191905.19+481506.2) — white dwarfs

1. INTRODUCTION

AM CVn systems are rare, ultra-compact, semi-detached, white dwarf binaries with periods ranging from 5 to 65 minutes. First identified over 40 years ago by Smak (1967), it has only been in the last decade that the number of known systems has risen above ten. Yet despite the recent discovery of almost 25 additional systems, their rich and complex phenomenological behavior has limited our understanding of this class of post-period minimum binaries. They are considered to be the helium analog of cataclysmic variables (CVs) and are important as strong, low-frequency Galactic gravitational wave sources (Nelemans et al. 2004; Roelofs et al. 2007b; Nissanke et al. 2012), the source of the proposed ".Ia" supernovae (Bildsten et al. 2007), and one of the believed end-points of binary white dwarf evolution (Nelemans et al. 2001). However, many questions about these unique systems remain, including their population density, their evolutionary pathways, and the interactions between the two components, including the He-rich accretion disk. We refer the reader to Nelemans (2005) and Solheim (2010) for general reviews.

Follow-up study of a newly-identify AM CVn system typically begins with a spectroscopic determination of its orbital period using phase-resolved spectroscopy of the "hot spot" (Nather et al. 1981), which is the location where matter from the donor hits the accretion disk. However, these measurements are incomplete, as the inclination of the systems cannot be determined. Only those systems showing eclipses and radial velocity variations of two components (e.g., the donor and accretor or the accretor and hot spot) allow for a full determination of the system's parameters (e.g., component masses, inclination, period, etc). Eclipses also allow for the extremely precise measurement of the orbital period change. For example, the orbital period of the double detached white-dwarf binary SDSSJ0651+2844 was measured to be decreasing by Hermes et al. (2012) while the only known eclipsing AM CVn system, SDSSJ0926+3624 (Anderson et al. 2005; Copperwheat et al. 2011, hereafter C11), was recently shown to have an increasing orbital period (Szypryt et al. 2014).

AM CVn systems have been observed to have three relatively distinct phenomenological states. Systems with orbital periods (hereafter P_{orb}) less than 20 min have been observed in a "high" state, characterized by optically thick accretion disks and absorption-line spectra. In contrast, systems with $P_{orb} > 40$ min, are observed to have emission-line spectra from what are believed to be optically-thin accretion disks and are said to be in quiescence (though see Woudt et al. 2013 for an example of a longer period system that has been observed to outburst). Systems in neither class show photometric variability over 0.5 mag.

Between these orbital period limits are outbursting systems, which are observed to have dwarf nova-type outbursts of 3–6 mag as well as variability at the 10% level in both quiescence and outburst (e.g., Patterson et al. 1997). Recent studies have shown that the frequency of these outbursts decreases as the orbital period increases (Levitan et al. 2011; Ramsay et al. 2012).

The population density of AM CVn systems has not been conclusively determined: population synthesis estimates of the space density (Nelemans et al. 2001) have not been observationally confirmed by color-selected samples (Roelofs et al. 2007b; Carter et al. 2013). The

[1] Division of Physics, Mathematics, and Astronomy, California Institute of Technology, Pasadena, CA 91125, USA.
[2] Department of Astrophysics/IMAPP, Radboud University Nijmegen, PO Box 9010, NL-6500 GL Nijmegen, the Netherlands.
[3] Department of Astronomy and Astrophysics, University of California, 1156 High Street, Santa Cruz, CA 95064, USA.
[4] Centre for Astronomy, School of Physics, National University of Ireland, Galway, Ireland.
[5] Spitzer Science Center, MS 314-6, California Institute of Technology, Pasadena, CA 91125, USA
[6] Benoziyo Center for Astrophysics, Faculty of Physics, Weizmann Institute of Science, Rehovot 76100, Israel
[7] GRANTECAN S.A. Cuesta de San José, s/n - 38712 - Breña Baja - La Palma, España.

latest results of Carter et al. (2013) suggest a space density of $(5 \pm 3) \times 10^{-7}\,\mathrm{pc}^{-3}$, a factor of 50 lower than the population synthesis estimates by Nelemans et al. (2001). The reason for this discrepancy is currently unknown. We note that these color-selected samples are mostly sensitive to longer period systems.

Over the last two years, we have conducted a search for outbursting AM CVn systems using the Palomar Transient Factory[8] (PTF; Law et al. 2009; Rau et al. 2009) large-area synoptic survey, in part, to use a different approach to the discovery of AM CVn systems that does not rely on their colors. The PTF uses the Palomar $48''$ Samuel Oschin Schmidt telescope to image up to $\sim 2,000\,\mathrm{deg}^2$ of the sky per night to a depth of $R \sim 20.6$ or $g' \sim 21.3$. After identifying outbursting systems, we obtain classification spectra. To date, this survey has identified >340 cataclysmic variables (CVs), six new AM CVn systems, and one extremely faint AM CVn candidate (Levitan et al. 2011, 2013).

In this paper, we present PTF1 J191905.19+481506.2 — a new AM CVn system discovered by the Palomar Transient Factory. This system is particularly interesting because:

- shallow eclipses are present, making it only the second known eclipsing AM CVn system.
- its orbital period is the shortest known of outbursting AM CVn systems.

We note that while this system is in the Kepler field, it, unfortunately, fell into a gap between the detectors of the *Kepler* satellite.

This paper is organized as follows. In Section 2 we discuss our data reduction and analysis methods. In Section 3 we present both short-term and long-term photometric and spectroscopic data and perform a period analysis. We consider the system's geometric structure and the rate of eclipsing AM CVn systems in Section 4. We summarize in Section 5.

2. DATA ACQUISITION, REDUCTION, AND ANALYSIS

2.1. *Photometric Data*

The initial discovery of PTF1 J191905.19+481506.2, hereafter PTF1J1919+4815, as an outbursting compact binary candidate was made using the PTF. Two pipelines process PTF data. The "transient" pipeline uses difference imaging to identify possible transients in real-time (Gal-Yam et al. 2011). In contrast, the "photometric" pipeline prioritizes photometric accuracy at the cost of processing time and uses aperture photometry to measure fluxes. This paper uses data from the latter.

The photometric pipeline applies standard de-biasing, flat-fielding, and astrometric calibration to raw images (Laher et al. 2014, submitted). Absolute photometric calibration to the few percent level is performed using a fit to SDSS fields observed in the same night (Ofek et al. 2012). Additional relative photometric calibration is applied to improve precision to 6–8 mmag at the bright end of $R \sim 14$ and 0.2 mag at the faint end of $R \sim 20.6$. This algorithm is described, in part, in Section 2.1.1.

While the initial identification of the system as an outbursting, compact binary candidate was done using data from the aforementioned pipeline, the crowded nature of the field requires point spread function (PSF) photometry for optimal results. We therefore re-processed the PTF images using the same pipeline as described in Section 2.1.1.

Dedicated long-term monitoring was obtained using the Palomar $60''$ (P60) telescope. The P60 automated pipeline, which includes automated de-biasing, flat-fielding, and astrometric calibration, is described in Cenko et al. (2006).

High-cadence observations were obtained from two sources. The first observations were made using the Lick 3-m Shane telescope with the Kast imaging spectrograph in imaging mode. We inserted a g' filter into the user filter wheel, replaced the dichroic with a mirror, and used a clear window instead of a grism. This provided an approximately $2' \times 2'$ field of view in a single filter with a dead time of 3.0 s between exposures utilizing the fast CCD read-out mode and disabling auto-erase of the CCD. Data were de-biased and flat-fielded using standard routines and astrometrically calibrated using the STARLINK package AUTOASTROM.

More recent high-cadence observations were obtained with the Caltech High speed Multi-color camERA[9] (CHIMERA), recently developed for the Palomar $200''$ (5.1 m) telescope's (P200) prime focus. Incoming light is split using a dichroic element onto two cameras, first passing through a g' filter on one side and an r' or i' filter on the other. The instrument can interchangeably make use of either Andor NEO sCMOS cameras or Andor iXon 897 Ultra EM-CCD cameras, depending on the requirements for each program (field of view, cadence, red versus blue response).

For this paper, we use only g' data captured by an Andor EM-CCD. This camera, when installed in CHIMERA, provides a $2' \times 2'$ field of view with $0.35''\,\mathrm{pixel}^{-1}$ plate scale. Exposures were de-biased and flat-fielded using standard routines. Photometric calibration was performed as described in Section 2.1.1, with the exception that the photometric measurements were made using the APPHOT package in IRAF.

2.1.1. *Photometric Calibration*

Photometric measurements for the PTF, P60, and Lick data presented here were made using PSF photometry as implemented by the AUTOPHOTOM package. Photometric calibration was performed for all photometric data using a least-squares matrix algorithm described in Ofek et al. (2011) and Levitan et al. (2011). The algorithm is similar to that in Honeycutt (1992), but allows for a simultaneous fit to reference magnitudes, providing both absolute and relative calibration in one step. The absolute calibration for this data was derived from USNO B-1.0, which is accurate to 0.5 mag (Sesar et al. 2006). We note that the same algorithm is used for the photometric PTF pipeline, except that the photometric PTF pipeline is based on photometric measurements from Sextractor (Bertin & Arnouts 1996).

2.2. *Spectroscopic Data*

[8] `http://ptf.caltech.edu/`

[9] for more information contact PI G. H., instrument scientist L. K. H. or see `http://tauceti.caltech.edu/chimera/`

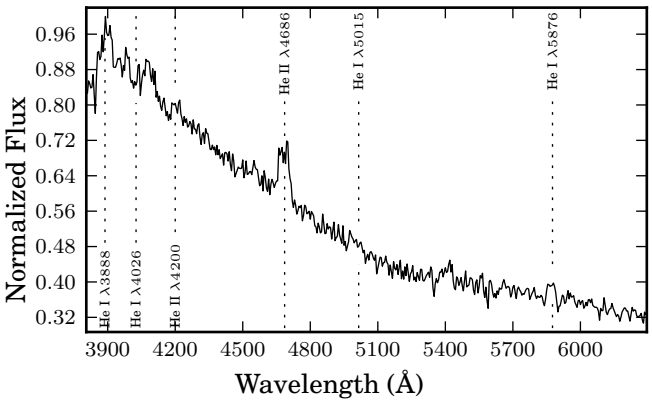

FIG. 1.— The classification spectrum of PTF1J1919+4815 obtained using the DBSP instrument on the Palomar 200″. Significant lines are identified. The absence of Balmer-series lines and the presence of He lines indicated that this was a likely AM CVn system. In contrast with the quiescent spectra of AM CVn systems, very few He I lines show significant emission, most notably He I λ5875, while He II λ4686 is very strong with an equivalent width of -11.4 ± 0.8Å.

Spectroscopic data were acquired from a number of telescopes and instruments; all were long-slit spectrographs. The observations are detailed in Section 3. The initial identification spectra obtained using the P200 were reduced using standard IRAF routines. All follow-up phase-resolved spectroscopic data were reduced using optimal extraction (Horne 1986) as implemented in the PAMELA code (Marsh 1989) as well as the STARLINK packages KAPPA, FIGARO, and CONVERT. Spectra obtained from the red side of Keck-I/LRIS were processed with L.A. COSMIC (van Dokkum 2001) due to the large number of cosmic rays.

2.3. *Period Estimation*

We use Lomb-Scargle periodograms (Scargle 1982; implementation by Richards et al. 2011) to identify periods in the data. Error estimation is performed using a bootstrap approach (Efron 1982). For each data set of length N points, we draw N points at random, allowing for repetition. We then generate a Lomb-Scargle periodogram for the selected points and find the peak. This method allows us to randomly vary both the length of the data set and the points from which a period is calculated. We repeat this process 500 times, and take their robust standard deviation, defined as $\sigma_{\rm rob} = 0.741(75^{\rm th}\ \text{percentile} - 25^{\rm th}\ \text{percentile})$, as an estimate of the error.

3. OBSERVATIONS AND PERIOD ANALYSIS

PTF1J1919+4815 was detected as a possible transient on 2011 July 11. A spectrum obtained at the Palomar 200″ (P200) on 2011 July 23, likely while the system was still in outburst, showed a strong He II 4686 emission line, but no other significant spectral lines (Figure 1). A second spectrum taken on 2011 August 03 detected the system while it was in a much fainter state, resulting in much lower signal-to-noise with few discernible lines. The combination of the crowded field (relative to the PTF's pixel scale of $1.01''\,{\rm pix}^{-1}$) and lack of a clear spectral signature led to the object being left for future study.

In 2011 December, PTF1J1919+4815 was identified as a candidate outbursting source as part of the PTF search for outbursting sources (Levitan et al. 2013). The combination of no Balmer lines and the presence of He II in the initial spectrum, as well as the outbursting behavior, led to its initial classification as an AM CVn system candidate. The likelihood that PTF1J1919+4815 was a short-period system made phase-resolved observations necessary to understand its nature.

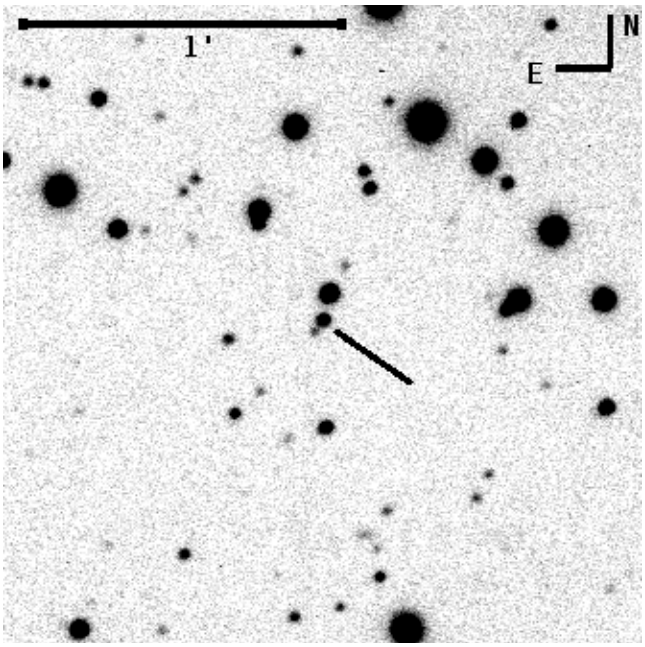

FIG. 2.— A $2' \times 2'$ finding chart of PTF1J1919+4815 based on a 5 min exposure with a g' filter obtained using the P200 while the system was in quiescence. The target is very close to two unrelated stars: a relatively bright star to the northwest and a very faint star to the southeast. The brighter neighbor is too far away to have a significant impact on the photometry, while careful flux extraction and the faint nature of the second neighbor should minimize any contamination.

Between 2012 May and 2013 April, we obtained both high speed photometry (Section 3.1) and phase-resolved spectroscopy (Section 3.2). Simultaneously, we began long-term photometric monitoring of PTF1J1919+4815 (Section 3.3). A summary of all non-PTF observations is presented in Table 1. A finding chart, useful given the crowded nature of the field, is shown in Figure 2. A long-term light curve of PTF1J1919+4815, indicating the times of the higher-cadence observations described below, is presented in Figure 3. Most data presented here are publicly available on the PTF website.

3.1. *High-cadence photometric observations*

The high-cadence photometric observations provide the most unambiguous measurements of PTF1J1919+4815's geometric configuration. In 2012 May, June, and July we obtained several series of exposures with the Lick 3-m Shane telescope using a g' filter and 15–30 s exposures (see Table 1). The 3-month baseline of these observations provides the best estimate for a period. However, the relatively long exposure times result in a poor time resolution relative to the short orbital period of AM CVn systems. Our more recent data set, from the P200 telescope with the CHIMERA instrument, has similar signal-to-noise per exposure but with only 5 s integrations and effectively no

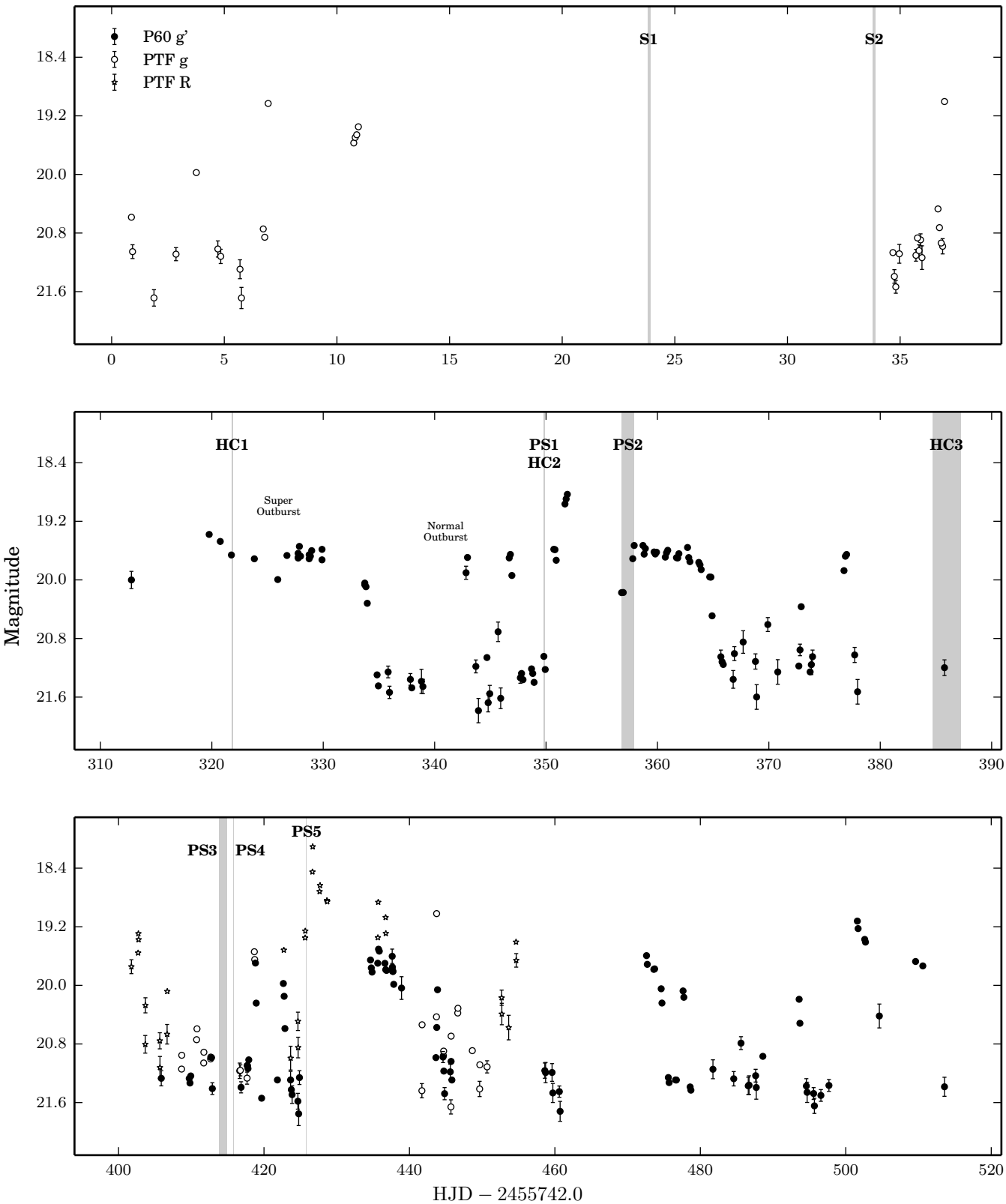

FIG. 3.— A long-term light curve of PTF1J1919+4815, with data from P60 g', PTF R-band, and PTF g'-band. Error bars are only shown for those detections with errors of greater than 0.075 mag. We label examples of a super outburst and a normal outburst. We also indicate the times of follow-up observations using highlighted areas and labels — HC indicates high-cadence photometry, S indicates a single spectrum, and PS indicates phase-resolved spectroscopy. More information on the follow-up observations is in Table 1.
The data from the three telescope and filter combinations were not jointly calibrated. Rather, all data were calibrated against an external source (USNO-B 1.0 B-band for g'-band observations and R-band for R observations) and for the g'-band data sets are very similar (within 10%). Given the large variability observed here, additional calibration was deemed to be unnecessary.

TABLE 1
Details of Selected Observations

Designation	UT Date	State[a]	Telescope	Setup	# of Exp.	Exp. Time (s)
S1	2011 Jul 22	Outburst	P200/DBSP	B: 600/4000, R: 158/7500	1	1200
S2	2011 Aug 02	Quiescence	P200/DBSP	B: 600/4000, R: 158/7500	1	900
S3	2012 Feb 01	Quiescence	P200/DBSP	B: 600/4000, R: 316/7500	1	1480
HC1	2012 May 16	Outburst	Lick/Kast	Imaging (g')	201	30
PS1	2012 Jun 13	Quiescence	Keck/LRIS	B: 600/4000, R: 600/7500	B: 81, R: 76	120
HC2	2012 Jun 13	Quiescence	Lick/Kast	Imaging (g')	203	30
PS2	2012 Jun 20	Outburst	GTC/Osiris	R1000B	40	120
···	2012 Jun 21	Outburst	GTC/Osiris	R1000B	21	120
HC3	2012 Jul 18	Quiescence	Lick/Kast	Imaging (g')	575	15
···	···	···	···	···	100	30
···	2012 Jul 19	Quiescence	Lick/Kast	Imaging (g')	55	30
···	2012 Jul 20	Quiescence	Lick/Kast	Imaging (g')	257	30
PS3	2012 Aug 16	Quiescence	Keck/LRIS	B: 600/4000, R: 600/7500	B: 75, R: 69	120
···	2012 Aug 17	Outburst	Keck/LRIS	B: 600/4000, R: 600/7500	B: 84, R: 78	120
PS4	2012 Aug 18	Quiescence	Gemini/GMOS-N	B600	103	125
PS5	2012 Aug 28	Outburst	Gemini/GMOS-N	B600	110	125
HC4	2013 Apr 04	Outburst	P200/CHIMERA	Imaging (g')	954	5

Note. — The telescopes/instruments referenced above are as follows:
Gemini/GMOS-N: Gemini North 8-m telescope with the GMOS-N imaging spectrograph (Hook et al. 2004).
GTC/OSIRIS: GranTeCan 10.4-m telescope with the OSIRIS imaging spectrograph (Cepa 1998).
Keck-I/LRIS: Keck-I 10-m telescope with the Low Resolution Imaging Spectrometer (Oke et al. 1995; McCarthy et al. 1998).
Lick/Kast: Shane telescope at the Lick Observatory with the Kast imaging spectrograph (Miller et al. 1988; Miller & Stone 1992).
P200/DBSP: Palomar 200″ telescope with the Double Spectrograph (Oke & Gunn 1982).
P200/CHIMERA: Palomar 200″ with the Caltech High-speed Multi-color CamERA (Section 2.1).

[a] Indicates the photometric state of the system between quiescence and outburst. We base this determination only on the rough photometric magnitude of the system at the time of observation.

dead time between exposures. This light curve is ideal for studying the intra-orbital photometric variability of PTF1J1919+4815, but its short length of only ∼1 hr precludes its use for a period determination. We use the CHIMERA data set to show the presence of an eclipse (Section 3.1.1) and the Lick data set to identify the precise orbital period (Section 3.1.2).

3.1.1. *CHIMERA Light Curve*

We present the CHIMERA light curve in Figure 4. At the time of observation, PTF1J1919+4815 was in outburst, and shows the characteristic superhumps seen in other outbursting AM CVn systems (e.g., Figure 4 of Wood et al. 2002). Superhumps are believed to be caused by deformation of the disk while the system is in outburst, and typically have periods a few percent longer than the orbital period (Warner 1995). The most prominent features noticeable besides the sawtooth shape of the superhumps are the three "dips" in luminosity for each orbit of PTF1J1919+4815. We now consider the nature of these dips.

We begin by considering the dip which occurs shortly before peak luminosity for each superhump cycle. If one were to remove the other two dips and draw a straight line from peak luminosity to minimum luminosity, then this last dip constitutes the minimum of the superhump sawtooth shape. Hence, we do not believe it to have a geometrical cause beyond the superhump phenomenon itself.

We now turn our attention to the remaining two dips. The presence of one dip with a ≤5% decrease (labeled as "superhump dip" in Figure 4) has been observed in other AM CVn systems (e.g., CR Boo and V803 Cen both show such features; Patterson et al. 1997, 2000), but its cause is unknown. However, a second decrease of any kind has not been observed in other systems except SDSSJ0926+3624 (C11), the first-discovered eclipsing AM CVn system. Hence, we tentatively conclude that the dip near the peak of the superhump is a feature intrinsic to the superhump itself, while the second dip is an eclipse of some localized emission on the disk, possibly the hot spot. This conclusion is supported by additional data we acquired from the Shane telescope, which we discuss in Section 3.1.2.

The CHIMERA light curve indicates only a single eclipse, with a relatively symmetric ingress and egress. We did consider the possibility that the third dip, which we earlier identified as part of the sawtooth pattern, is an eclipse of the hot spot, making the earlier dip an eclipse of the white dwarf. However, the separation of ∼4 min between these two dips means that the donor would have to eclipse the hot spot at an orbital phase offset of ∼0.2, something that is highly unlikely.

In addition to the prominent dips, we also highlight the presence of significant variability on the 1–2 min timescale, particularly immediately after the superhump dip. The source of this variability is unknown and further observations are necessary to ensure that it is, in fact, real. If so, it may be related to the flickering phenomenon seen in CVs (Bruch 1992).

3.1.2. *Lick Light Curves*

The data we obtained from the Lick Shane telescope, while of coarser time resolution, are particularly useful for period analysis due to its long baseline. We present light curves, Lomb-Scargle periodograms, and folded light curves in Figures 5 and 6 for the nights of 2012 May 16 and 2012 July 20, respectively. For the data from each night, we subtracted a first order linear fit to remove any linear trend. The remaining nights show similar characteristics to these, and are both included in the overall period analysis in Section 3.1.3. All light curves are available on the PTF website.

Both the 2012 May and 2012 July data show variability with an amplitude of ∼0.15 mag, including both a small increase in luminosity as well as the eclipse feature. The eclipse is of similar depth to that seen in the CHIMERA data. We believe that the luminosity increase in the 2012 July data is a result of the hotspot rotating into view, as has been shown for CVs (e.g., OY Car; Schoembs & Hartmann 1983) and AM CVn systems. Levitan et al. (2011) explicitly showed the link between the hot spot and the variability for PTF1J0719+4858, but the variability in quiescence has been observed in several AM CVn systems (e.g., Patterson et al. 1997; Wood et al. 2002).

The origin of the 2012 May variability is more difficult to determine. PTF1J1919+4815 was in outburst at the time the data were obtained (see Figure 3) and this would typically indicate the presence of superhumps (as seen in the CHIMERA data; see Section 3.1.1). Superhumps, however, typically have a period slightly longer than the orbital period (Patterson et al. 2005) and hence should be out of phase with the eclipse. We note that WZ Sge, a CV which also shows only a disk eclipse, has shown significant differences in eclipse shape between outburst and quiescence (Patterson et al. 2002). Given the faintness of PTF1J1919+4815 in quiescence, we do not have sufficient signal-to-noise to clearly see any such differences in this system.

In this case, the eclipse in the 2012 May data is at the same phase with respect to the luminosity increase as in the 2012 July data. With fewer than two hours of data, it is impossible to measure the period of the variability with sufficient precision to distinguish between the orbital period and any slightly longer superhump period. Hence, we cannot say whether this variability is from the hot spot (thus indicating the lack of superhumps for part of the outburst; see, e.g., C11) or a chance superposition of the orbital period and the superhump period (as can be seen, for example, in Figure 3 of C11 for SDSSJ0926+3624).

We now consider the origin of the observed eclipse. The accretor is believed to be significantly more compact than the donor and contributes the majority of the luminosity of at least some AM CVn systems (e.g., Bildsten et al. 2006; C11). Any eclipse of the accretor would likely have a sharp ingress and egress and a depth of greater than 10% (as observed for PTF1J1919+4815). This leaves only a localized area of emission on the disk as a possible explanation. It is likely that this is the hot spot typically observed for semi-detached binaries, particularly for the data taken in quiescence. However, we are cautious about concluding that all data, including that taken in outburst, shows an eclipse of the hot spot as opposed to some other disk feature, as it is believed that the superhump phenomena results in a somewhat more extended area of disk emission (Simpson & Wood

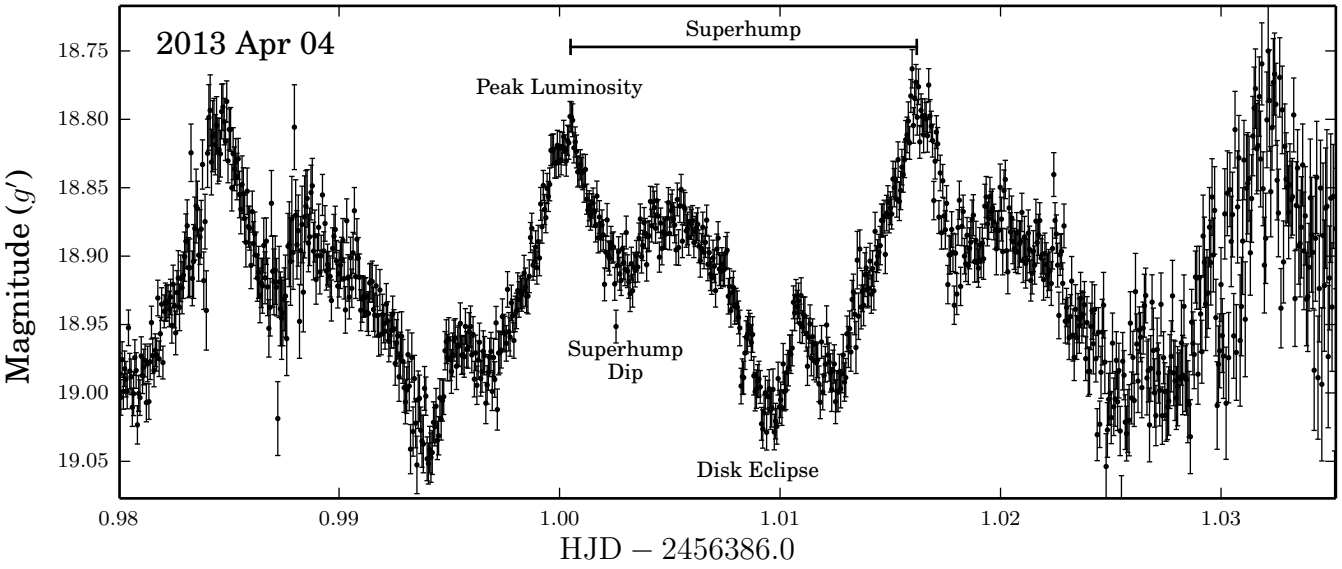

FIG. 4.— The light curve of PTF1J1919+4815 taken using the CHIMERA instrument on 2013 Apr 4. The high time resolution (5 s exposures and effectively no dead time between exposures) resolves many features of the photometric variability; prominent features are labeled. PTF1J1919+4815 was in outburst at the time of observation, and thus shows a superhump structure as well as the eclipse of the disk. The increased scatter towards the end of the observations is due to the brightening sky.

1998).

3.1.3. *Orbital Period Analysis*

We stress that while the eclipse feature is certainly not strong, it is stable and repeating over data sets obtained with two different telescopes and over a time span of over 10 months, as well as in both quiescent and outburst states of PTF1J1919+4815. We thus conclude that this is an eclipse of the hot spot and proceed with a period analysis.

Outbursting AM CVn systems have been observed to show photometric variability at two periods, one in outburst (from the superhumps) and one in quiescence (likely from the hot spot; Levitan et al. 2011). We begin our analysis with the 2012 July data, which, being in quiescence, should show variability at the orbital period of the system. The best periods obtained from the individual light curves were 22.41 ± 0.09 min and 22.44 ± 0.11 min for the nights of 2012 July 18 and 2012 July 20, respectively. If we analyze all the 2012 July data simultaneously, we find a best period of 22.46 ± 0.09 min. Finally, if we analyze all data from 2012 May, June, and July simultaneously, we find a best period of 22.4559(3) min. All errors are calculated from bootstrap simulations, as described in Section 2.3. The times used in all calculations are based on the local time stamps provided by the Kast instrument, offset to UTC time, and subsequently corrected for light-travel time by conversion to HJD. We note that the error estimates of the period do not change linearly with respect to the baseline, as might be expected. This may be due to slight changes in the light curve between nights, perhaps similar to that seen for WZ Sge (Patterson et al. 2002). Lastly, the closest alias is at 22.4671 min, which is 37σ from the best period and shows no eclipse in a phase-binned light curve.

The long exposure times used, the weakness of the eclipse, and the faint nature of the system make ephemeris determination non-trivial. To obtain an estimate with an accurate error estimate, we used a matched filter technique. For our template, we selected a triangular function of width 3.7 min and depth 0.1 mag (roughly consistent with the shape of the eclipse). We calculated the cross-correlation of the template with the light curve using a $\Delta t = 1$ s and identified the maxima of this function for each orbital period. We limited the data used to that from 2012 May 16, the first half of 2013 Jul 18, and 2013 Jul 20. If the remainder of the data is included, the resulting ephemeris does not change significantly, but the error, calculated based on the scatter of the observed minima with the predicted minima, is significantly higher due to poorer conditions in that data.

Given the agreement in the periods measured from these light curves, we propose 22.4559(3) min as the orbital period of PTF1J1919+4815 and an ephemeris of

$$HJD = 2456063.8650(5) + 0.0155944(2)E$$

for the mid-point of the eclipse. We acknowledge that the error measurement of the orbital period may be overly optimistic, as it is from a bootstrap simulation and does not include systematic errors. However, it is consistent with the long baseline of observations and when all data are folded at this period, the eclipse is clearly visible (Figure 7).

3.2. *Phase-resolved Spectroscopy*

We obtained phase-resolved spectroscopy on six separate nights, although the outburst state was different for almost every one of these nights (see Figure 3 and Table 1). For each night, we co-added the flux around several He emission lines in velocity space and folded the spectra on the orbital period identified in Section 3.1.3. However, no clear "S-wave" was observed, as would be expected for an AM CVn system (Nather et al. 1981). Likewise, a search for an orbital period in this data did not yield any discernible orbital period. We present one of these trailed, phase-folded spectra in Figure 8.

Next, we generated Doppler tomograms (Marsh & Horne 1988) using multiple emission lines (which pro-

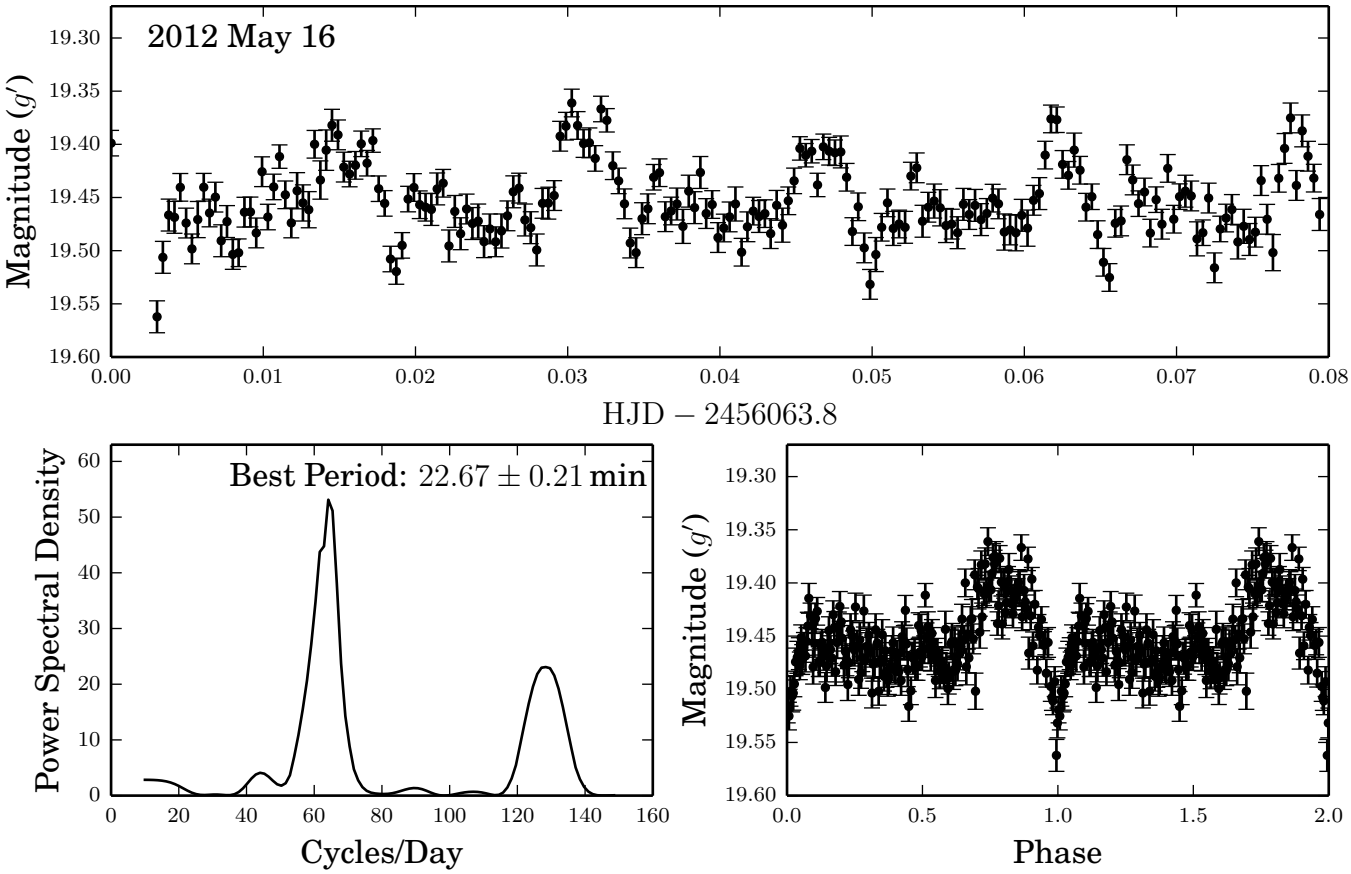

FIG. 5.— A high-cadence light curve of PTF1J1919+4815 observed by the Lick 3-m on 2012 May 16. The top panel is the light curve, the bottom-left panel is a periodogram of the light curve, and the bottom-right panel is the light curve folded on the orbital period proposed in Section 3.1.3. The eclipse is at a phase of 0.0 using the ephemeris calculated in the same section. The eclipse is clearly visible in the data presented here. It is unknown whether the variability is due to superhumps or the hot spot.

vides for better signal to noise in faint, shorter period systems — see Kupfer et al. 2013 for an example). The tomogram should boost the signal of the hot spot since all light is concentrated at one point in velocity space, yet we did not see any strong hot spot in any of the Doppler tomograms (Figure 8).

The lack of a clear signal in the trailed, phase-folded spectra and the Doppler tomograms is mysterious. We do not attribute this to a lack of data, as Levitan et al. (2013) found a faint S-wave in a $g' > 22$ AM CVn system with a similar amount of data as what we obtained for PTF1J1919+4815. Time variability of the visibility of the hot spot has been observed for other AM CVn systems (Roelofs et al. 2009) and may be the reason we could not identify an S-wave in the data. We thus conclude that the hot spot in PTF1J1919+4815 had lower contrast with the accretion disk than in other systems during the times it was observed, but note that this does not change our conclusions about the orbital period, as no clear signal was found in the spectroscopic data and the photometric signal is much less ambiguous.

3.3. *Long-term Photometric Variability*

We explore the long term photometric variability of PTF1J1919+4815 using the 355 photometric measurements over ∼200 d. We identify the presence of super-outbursts and the much shorter normal outbursts. The latter, in particular, appear to last ∼1 d and were observed to occur 2–3 times between super-outbursts, consistent with CR Boo (Kato et al. 2000) and PTF1J0719+4858 (Levitan et al. 2011), both of which have similar orbital periods as PTF1J1919+4815.

Our data covers approximately 5 super-outburst cycles and these super outbursts are seen to recur every ∼35 d. We use a periodogram of the P60 data to calculate the strongest period of 36.8 ± 0.8 d. Folding the light curve (see Figure 9) at this period results in a remarkably well-defined super-outburst light curve, something that is not seen in most AM CVn systems. We note that we use the periodogram itself only to refine the already evident recurrence time.

This super-outburst recurrence time is slightly shorter than that observed for CR Boo, which has an orbital period of 24.5 min. The duration of the super-outburst is ∼13 d and its amplitude (peak luminosity minus quiescent luminosity) is ∼3 mag. Although the data shown here indicates regular super-outbursts, long-term study of CR Boo (Honeycutt et al. 2013) suggests that this is likely to only be a temporary state. Moreover, with only 5 observed super-outbursts, the scatter in the super-outburst recurrence time measured here is likely to be underestimated as most AM CVn systems show changes of up to 15% (see, e.g., Ramsay et al. 2012).

3.4. *Median Spectra and Long-term Variability*

AM CVn systems are known to have significant changes in their spectra corresponding to their different states. PTF1J1919+4815, with its frequent changes between

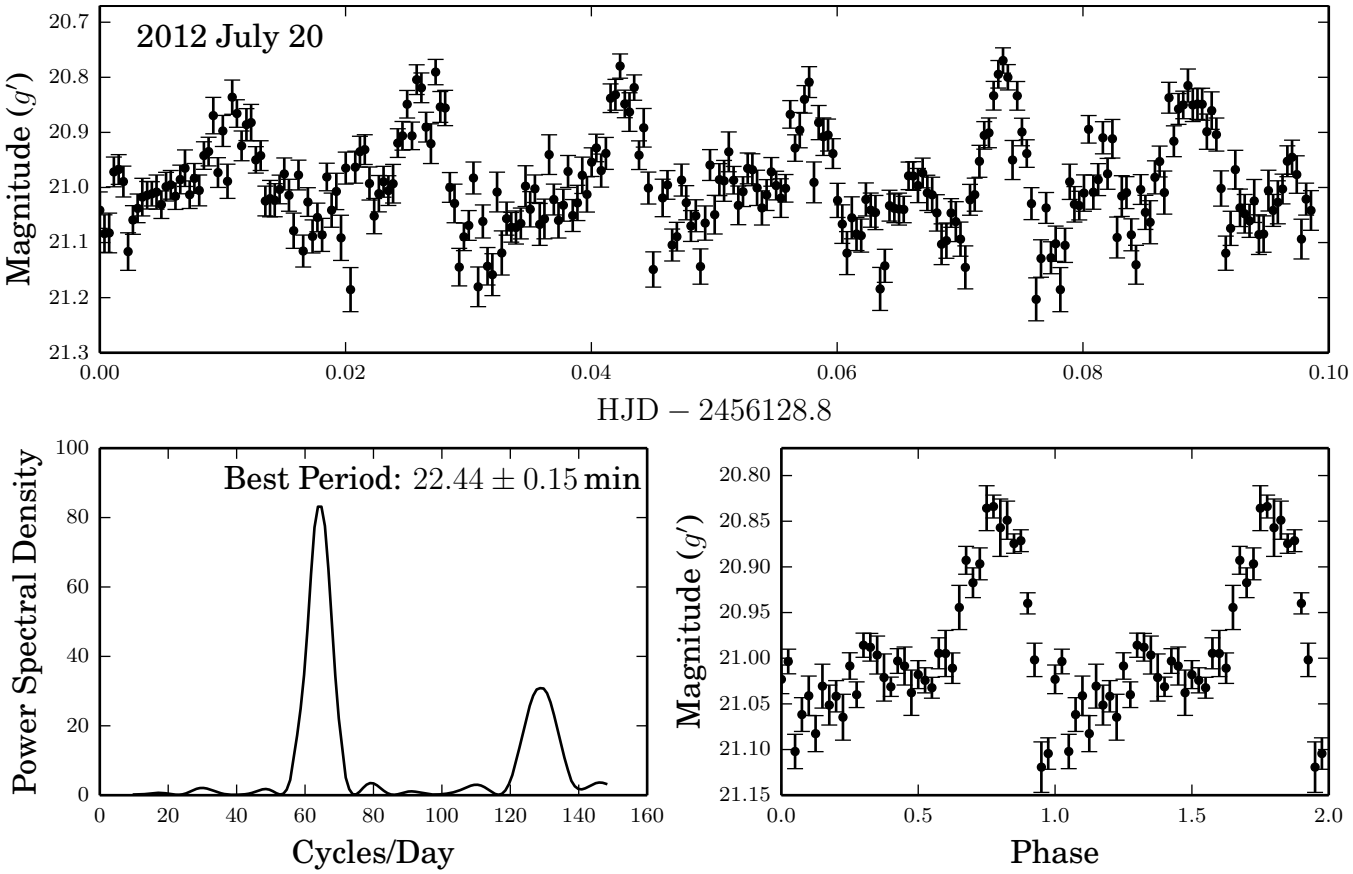

FIG. 6.— A high-cadence light curve of PTF1J1919+4815 observed by the Lick 3-m. This light curve is from 2012 July 20. The top panel is the light curve, the bottom-left panel is a periodogram generated from the light curve, and the bottom-right panel is the light curve phased-binned at the orbital period proposed in Section 3.1.3. The eclipse is at a phase of 0.0 using the ephemeris calculated in the same section. This light curve was taken while the system was in quiescence, and shows the quiescent variability seen in other systems and believed to be directly related to the orbital period (Levitan et al. 2011). The data from 2012 July 18 and 19 are similar.

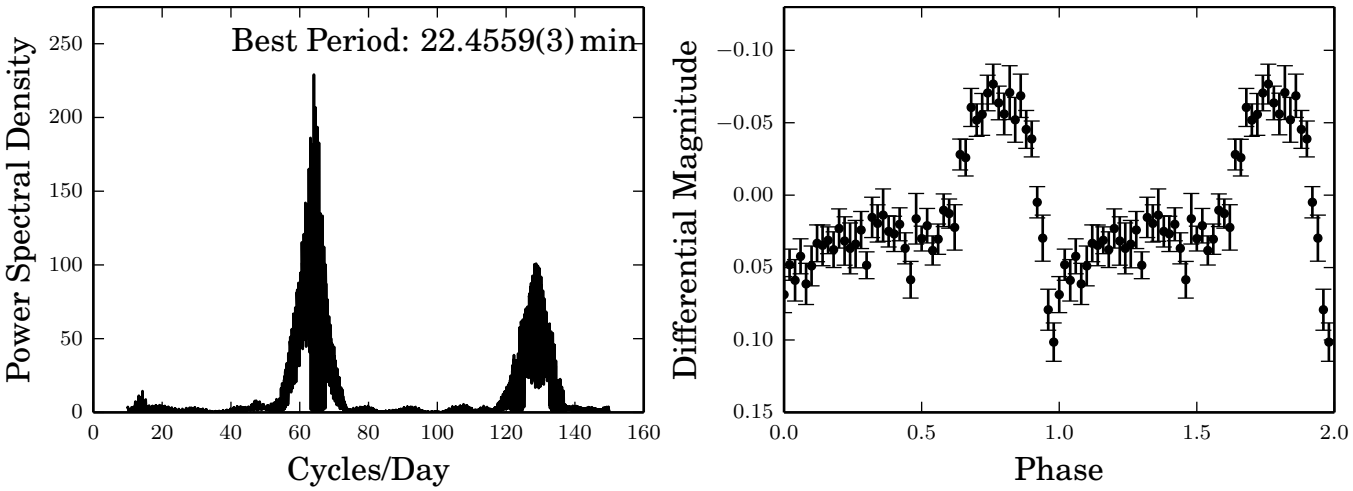

FIG. 7.— A periodogram and phase-binned light curve of all observations of PTF1J1919+4815 on the Lick-3m. The light curve is folded at a period of 22.4559 min, the highest peak in the periodogram, and we plot the eclipse at a phase of 0.0 using the ephemeris as described in Section 3.1.3. The error bars on the light curve are the sample standard deviation of the measurements in each phase bin.

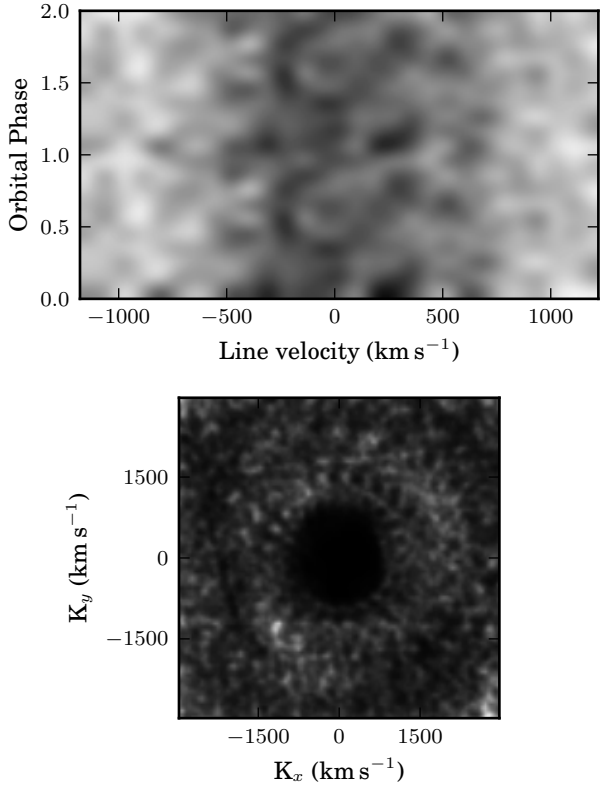

FIG. 8.— **Top:** The trailed, folded spectra from 2012 June 13 and 2012 August 16 folded at a period of 22.456 min. The He I $\lambda\lambda 4387, 4471, 4921,$ and 5015 lines were used. Unlike other AM CVn systems, no strong S-wave is present.
Bottom: Doppler tomogram generated from data taken on 2012 June 13 using the He I $\lambda\lambda 3888, 4026, 4921,$ and 5015 lines and the He II $\lambda 4686$ line. Doppler tomograms re-project spectroscopic data into Keplerian-velocity space — all flux from areas moving with the same velocity will be projected onto the same spot on the tomogram. This allows us to look for features such as a hot spot that would be at one velocity. No significant hot spot is seen in this tomogram, unusual for an AM CVn system.

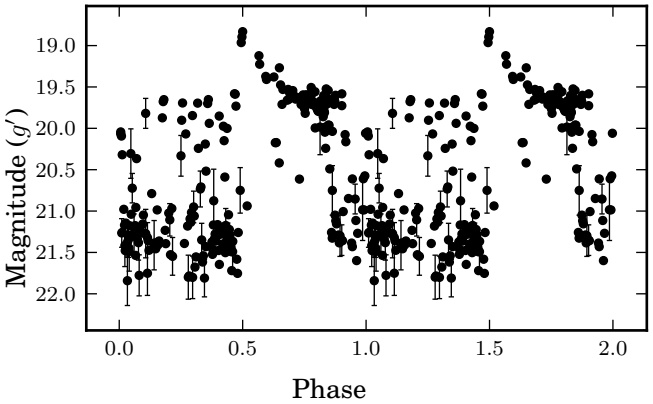

FIG. 9.— A light curve of the long-term P60 photometry folded at a period of 36.8 d. The folded light curve shows a very consistent super-outburst over the 5 super-outburst cycles (∼200 d) observed. The normal outbursts, however, do not coincide with each other. Some evidence is present for "dips" during the middle of the super-outburst, as reported by (Ramsay et al. 2012). However, the dips seen here are non-coherent, and it is unknown if these dips are related to those seen by Ramsay et al. (2012). The peak of the super-outburst is set to a phase of 0.5.

TABLE 2
EQUIVALENT WIDTHS OF PROMINENT LINES

Line	Quiescence (Å)	Outburst (Å)
He I 3705	... [a]	4.4 ± 0.2
He I 3819	-2.7 ± 0.5	3.9 ± 0.2[b]
He I 3888	-4.9 ± 0.4	
He I 3964	-1.1 ± 0.4	6.8 ± 0.2[c]
He I 4026	... [a]	
He I 4120/4143	X	4.4 ± 0.2
He I 4388	-0.5 ± 0.4	1.5 ± 0.1
He I 4471	-2.2 ± 0.4	3.3 ± 0.2
He II 4685	-3.4 ± 0.4[d]	-0.5 ± 0.1
He I 4713		... [a]
He I 4921	... [a]	2.8 ± 0.2
He I 5015	-3.6 ± 0.4	1.8 ± 0.2
He I 5875	-2.7 ± 0.6	1.9 ± 0.3
He I 6678	2.6 ± 0.5	... [e]
He I 7065	-2.1 ± 0.5	X

NOTE. — Quiescent equivalent widths are measured from the medium spectrum taken on 2012 August 16. Outburst equivalent widths are measured from the median spectrum taken on 2012 August 17. An X indicates that the line is not detectable above the noise level of the spectrum obtained.

[a] Line present but insufficient S/N to measure.
[b] Combined equivalent width of He I 3819 and He I 3888.
[c] Combined equivalent width of He I 3964 and He I 4026.
[d] Combined equivalent width of He II 4685 and He I 4713.
[e] Line present but contaminated with atmosphere.

outburst and quiescence, provides a good opportunity to consider the changes in spectra. In Figure 10 we present median spectra from three nights. In particular, these spectra show the evolution of the spectrum from the emission-line spectrum that AM CVn systems exhibit in quiescence (the 2012 June 13 spectrum) to the outburst spectrum showing absorption lines (the 2012 June 20 spectrum). The figure also shows the spectrum taken on 2012 August 28, at the start of a super-outburst (see Figure 3), which shows a distinct lack of features. We present equivalent widths of the significant lines identified in the outburst and quiescent spectra in Table 2.

4. DISCUSSION

Although the presence of the disk eclipse allows for a precise period estimate for such a faint system, the lack of an accretor eclipse precludes a full solution of the system structure. It also prevents us from measuring any change in the orbital period for this system, as the uncertainty on the disk radius and its likely change due to the presence of outbursts will overwhelm any expected change due to orbital evolution. However, the presence of the disk eclipse does allow us to estimate the inclination of the system if we make certain assumptions about the masses and radii of the two components.

Only one AM CVn system, SDSSJ0926+3624 (P_{orb} = 28.558 min; C11), has been observed to have eclipses of the accretor: and as a result, has had a full system solution derived. Here, we assume that the evolutionary origin and, hence, system properties of PTF1J1919+4815 are similar to that of SDSSJ0926+3624. We caution that AM CVn systems are believed to have several possible evolutionary pathways (Nelemans et al. 2001) and that no conclusive evidence has been found that can differentiate a system's origin (Roelofs et al. 2007a; Nelemans et al. 2010).

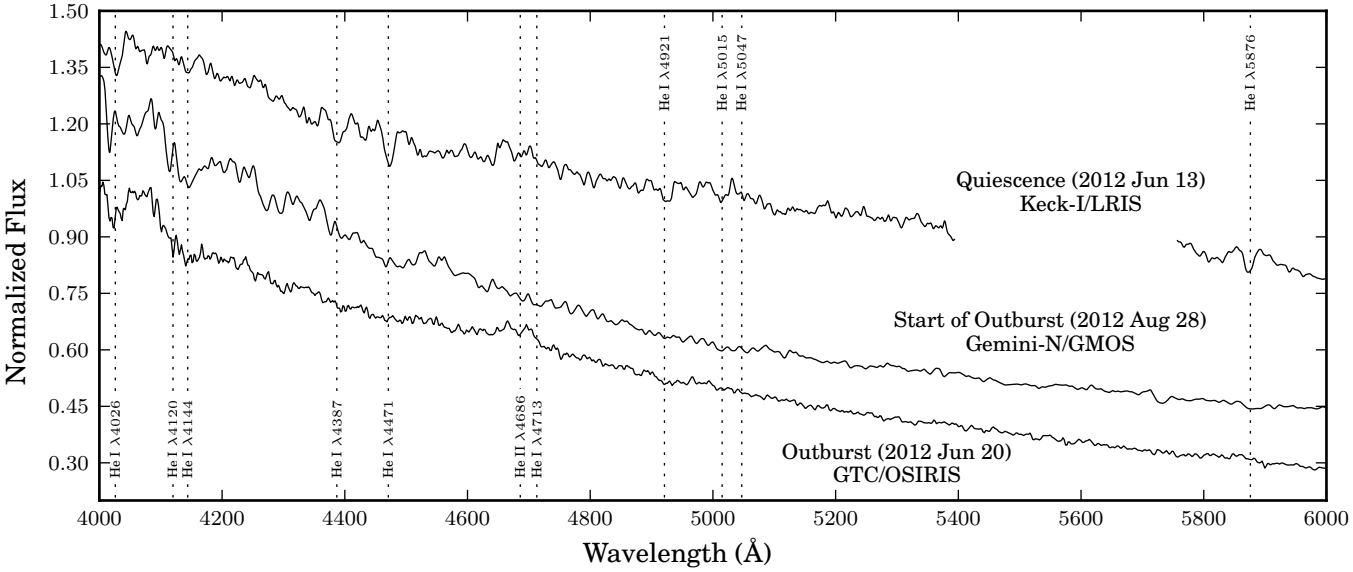

FIG. 10.— The median spectra from three nights: 2012 June 13, 2012 August 28, and 2012 June 13, arranged in this order from top to bottom. The flux of the first two spectra is shifted, respectively, 0.4 and 0.2 upwards from their normalizations. The most prominent He emission lines are shown. The first spectrum is of the system in quiescence and shows the He emission lines that AM CVns are known for. The other spectra are from the outburst state—in particular, the second spectrum shows few features and is from the initial rise to outburst, while the third spectrum is from the plateau phase and shows the absorption line features that have been observed for other systems in outburst.

From C11, the parameters of SDSSJ0926+3624 are: $M_1 = 0.85M_\odot$, $M_2 = 0.035M_\odot$, $R_1 = 9.7 \times 10^{-3}R_\odot$, and $q = M_2/M_1 = 0.041$. We use these values for PTF1J1919+4815, despite the difference in orbital period. Assuming standard mass transfer, only $\sim 0.01M_\odot$ would have been transferred during the evolution between the orbital periods of PTF1J1919+4815 and SDSSJ0926+3624, which is certainly below the uncertainties of the systems' respective evolutionary histories. Similarly, we adopt the radius of the accretor from SDSSJ0926+3624 to be that of the accretor in PTF1J1919+4815. The donor's radius will be that of the Roche Lobe as a first estimate, at the given period for the given mass ratio. Using the assumed masses for PTF1J1919+4815 and its orbital period with the approximation in Eggleton (1983), we find that the orbital separation, a, and the Roche-lobe radius, r_L, are $a = 0.25R_\odot$, and $r_L = 0.039R_\odot$. The last measurement needed is the radius of the disk. Based on the measurements of SDSSJ0926+2624, we assume a disk radius of $R_{disk} \approx 0.35a$. The derived values in C11 vary between observing runs, and since the size of the disk is expected to change between outburst and quiescence, we believe this is a reasonable, first assumption. We can constrain the inclination by determining for which inclinations the shadow of the donor star (as seen from Earth) passes over the hot spot, assumed to be a point source, but not the accretor. Combining the radii of disk, donor, and accretor, we can constrain the inclination to $76^\circ < i < 79^\circ$. We present a summary of system properties in Table 3.

Given the uncertainty in the system properties used, we consider the impact of several parameters on the results. The upper limit on i is primarily related to the accretor and donor masses. However, their masses are constrained by the initial conditions of AM CVn system formation and as such are not likely to change significantly even with moderate changes of the initial masses.

TABLE 3
SYSTEM PROPERTIES

U^a	19.814 ± 0.048
g^a	20.155 ± 0.016
r^a	20.522 ± 0.065
i^a	20.409 ± 0.121
Orbital period	22.4559(3) min
Super-outburst Recurrence Time	36.8 ± 0.4 d
Super-outburst Strength	$\sim$3 mag
Super-outburst Duration	$\sim$13 d
Inclination[b]	$74^\circ < i < 78^\circ$

[a] Photometric measurements are from the Kepler INT Survey DR2 (Greiss et al. 2012a,b) and are typical of the quiescent values for the system.
[b] These values assume that the radius of the accretion disk, $R_{disk} = 0.35a$, where $a = 0.25R_\odot$. See Section 4 for further details.

The lower bound, however, is significantly affected by the radius of the disk. If, for example, the radius of the disk was $0.5a$, the lower bound would drop to 72°. Had the inclination been greater than the upper limit here, an eclipse of the white dwarf should have been observable. Conversely, an inclination of less than the lower limit would result in no eclipse of either the hot spot or the accretor.

4.0.1. *Number of Eclipsing AM CVn Systems*

One peculiarity of the currently known population of AM CVn systems is the relative scarcity of eclipsing examples. In Section 4, we constrained the inclination of PTF1J1919+4815 to the range $76^\circ < i < 79^\circ$. This indicates that in $\sim$19% of systems with similar orbital periods the accretor should be eclipsed, and an additional $\sim$5% of similar systems should show an eclipse of the hot spot only, as is the case here. These calculations assume a random distribution of inclinations and an observed inclination distribution of $\sin(i)$. We note that longer

orbital period systems will have a smaller q and hence a lower probability of eclipse.

With the number of AM CVn systems rapidly approaching 40, it is somewhat surprising that only one system has shown an eclipse of the accretor and only one other a partial eclipse. The rate of observed eclipsing systems, ∼5% is lower than would be expected, even assuming that only 15% of systems are eclipsing (based on $q = 0.02$ for longer period systems). Even accounting for small-number statistics, one would expect at least 3 fully eclipsing systems. We do note that many long period systems do not have high-cadence photometric follow-up, but only time-resolved spectroscopy. However, a prominent eclipse should also show up in time-resolved spectroscopy through flux and/or line-strength/shape changes.

5. CONCLUSIONS

We have established PTF1J1919+4815 as an eclipsing AM CVn system from its He-rich and H-deficient spectrum, its phenomenological behavior, and its photometrically determined period. Its orbital period was measured to be 22.4559(3) min, but we did not find a significant hot spot in the S-wave and Doppler map. PTF1J1919+4815 shows a well-defined super-outburst that is 36.8 ± 0.4 d. Such a non-variable recurrence time is atypical for AM CVn systems. We used these measurements to constrain the inclination of the systems given assumptions about its evolution and to consider the geometric structure of the system.

T. K. acknowledges support by the Netherlands Research School of Astronomy (NOVA). We thank Dong Xu for reducing the initial classification spectra.

Observations obtained with the Samuel Oschin Telescope at the Palomar Observatory as part of the Palomar Transient Factory project, a scientific collaboration between the California Institute of Technology, Columbia University, Las Cumbres Observatory, the Lawrence Berkeley National Laboratory, the National Energy Research Scientific Computing Center, the University of Oxford, and the Weizmann Institute of Science. Some of the data presented herein were obtained at the W.M. Keck Observatory, which is operated as a scientific partnership among the California Institute of Technology, the University of California and the National Aeronautics and Space Administration. The Observatory was made possible by the generous financial support of the W.M. Keck Foundation. The authors wish to recognize and acknowledge the very significant cultural role and reverence that the summit of Mauna Kea has always had within the indigenous Hawaiian community. We are most fortunate to have the opportunity to conduct observations from this mountain. Based in part on observations obtained at the Gemini Observatory, which is operated by the Association of Universities for Research in Astronomy, Inc., under a cooperative agreement with the NSF on behalf of the Gemini partnership: the National Science Foundation (United States), the National Research Council (Canada), CONICYT (Chile), the Australian Research Council (Australia), Ministério da Ciência, Tecnologia e Inovação (Brazil) and Ministerio de Ciencia, Tecnología e Innovación Productiva (Argentina). The Gemini data were obtained under Program ID GN-2012B-Q-110. Based in part on observations made with the Gran Telescopio Canarias (GTC) installed in the Spanish Observatorio del Roque de los Muchachos of the Instituto de Astrofísica de Canarias, on the island of La Palma.

Facilities: PO:1.2m, PO:1.5m, Gemini:Gillett (GMOS-N), GTC (OSIRIS), Hale (CHIMERA), Hale (DBSP), Keck:I (LRIS), Shane (Kast Double spectrograph)

REFERENCES

Anderson, S. F., et al. 2005, AJ, 130, 2230
Bertin, E., & Arnouts, S. 1996, A&AS, 117, 393
Bildsten, L., Shen, K. J., Weinberg, N. N., & Nelemans, G. 2007, ApJ, 662, L95
Bildsten, L., Townsley, D. M., Deloye, C. J., & Nelemans, G. 2006, ApJ, 640, 466
Bruch, A. 1992, A&A, 266, 237
Carter, P. J., et al. 2013, MNRAS, 429, 2143
Cenko, S. B., et al. 2006, PASP, 118, 1396
Cepa, J. 1998, Ap&SS, 263, 369
Copperwheat, C. M., et al. 2011, MNRAS, 410, 1113
Efron, B. 1982, The Jackknife, the Bootstrap and other resampling plans (Philadelphia: Society for Industrial and Applied Mathematics)
Eggleton, P. P. 1983, ApJ, 268, 368
Gal-Yam, A., et al. 2011, ApJ, 736, 159
Greiss, S., et al. 2012a, AJ, 144, 24
—. 2012b, ArXiv e-prints, 1212.3613
Hermes, J. J., et al. 2012, ApJ, 757, L21
Honeycutt, R. K. 1992, PASP, 104, 435
Honeycutt, R. K., Adams, B. R., Turner, G. W., Robertson, J. W., Ost, E. M., & Maxwell, J. E. 2013, PASP, 125, 126
Hook, I. M., Jørgensen, I., Allington-Smith, J. R., Davies, R. L., Metcalfe, N., Murowinski, R. G., & Crampton, D. 2004, PASP, 116, 425
Horne, K. 1986, PASP, 98, 609
Kato, T., Nogami, D., Baba, H., Hanson, G., & Poyner, G. 2000, MNRAS, 315, 140
Kupfer, T., Groot, P. J., Levitan, D., Steeghs, D., Marsh, T. R., Rutten, R. G. M., & Nelemans, G. 2013, MNRAS, 432, 2048
Laher, R., et al. 2014, submitted, PASP
Law, N. M., et al. 2009, PASP, 121, 1395
Levitan, D., et al. 2011, ApJ, 739, 68
—. 2013, MNRAS, 430, 996
Marsh, T. R. 1989, PASP, 101, 1032
Marsh, T. R., & Horne, K. 1988, MNRAS, 235, 269
McCarthy, J. K., et al. 1998, Proc. SPIE, 3355, 81
Miller, J., & Stone, R. 1992, The CCD Cassegrain Spectrograph at the Shane Reflector, Tech. Rep. 48, Santa Cruz:Lick Observatory
Miller, J. S., Robinson, L. B., & Goodrich, R. W. 1988, in Instrumentation for Ground-Based Optical Astronomy, ed. L. B. Robinson, 157
Nather, R. E., Robinson, E. L., & Stover, R. J. 1981, ApJ, 244, 269
Nelemans, G. 2005, in ASP Conf. Ser., Vol. 330, The Astrophysics of Cataclysmic Variables and Related Objects, ed. J.-M. Hameury & J.-P. Lasota (San Francisco: ASP), 27
Nelemans, G., Portegies Zwart, S. F., Verbunt, F., & Yungelson, L. R. 2001, A&A, 368, 939
Nelemans, G., Yungelson, L. R., & Portegies Zwart, S. F. 2004, MNRAS, 349, 181
Nelemans, G., Yungelson, L. R., van der Sluys, M. V., & Tout, C. A. 2010, MNRAS, 401, 1347
Nissanke, S., Vallisneri, M., Nelemans, G., & Prince, T. A. 2012, ApJ, 758, 131

Ofek, E. O., Frail, D. A., Breslauer, B., Kulkarni, S. R., Chandra, P., Gal-Yam, A., Kasliwal, M. M., & Gehrels, N. 2011, ApJ, 740, 65
Ofek, E. O., et al. 2012, PASP, 124, 62
Oke, J. B., & Gunn, J. E. 1982, PASP, 94, 586
Oke, J. B., et al. 1995, PASP, 107, 375
Patterson, J., Walker, S., Kemp, J., O'Donoghue, D., Bos, M., & Stubbings, R. 2000, PASP, 112, 625
Patterson, J., et al. 1997, PASP, 109, 1100
—. 2002, PASP, 114, 721
—. 2005, PASP, 117, 1204
Ramsay, G., Barclay, T., Steeghs, D., Wheatley, P. J., Hakala, P., Kotko, I., & Rosen, S. 2012, MNRAS, 419, 2836
Rau, A., et al. 2009, PASP, 121, 1334
Richards, J. W., et al. 2011, ApJ, 733, 10
Roelofs, G. H. A., Groot, P. J., Benedict, G. F., McArthur, B. E., Steeghs, D., Morales-Rueda, L., Marsh, T. R., & Nelemans, G. 2007a, ApJ, 666, 1174
Roelofs, G. H. A., Nelemans, G., & Groot, P. J. 2007b, MNRAS, 382, 685
Roelofs, G. H. A., et al. 2009, MNRAS, 394, 367
Scargle, J. D. 1982, ApJ, 263, 835
Schoembs, R., & Hartmann, K. 1983, A&A, 128, 37
Sesar, B., et al. 2006, AJ, 131, 2801
Simpson, J. C., & Wood, M. A. 1998, ApJ, 506, 360
Smak, J. 1967, Acta Astron., 17, 255
Solheim, J. 2010, PASP, 122, 1133
Szypryt, P., et al. 2014, MNRAS, in press
van Dokkum, P. G. 2001, PASP, 113, 1420
Warner, B. 1995, Cataclysmic variable stars (Cambridge: Cambridge University Press)
Wood, M. A., Casey, M. J., Garnavich, P. M., & Haag, B. 2002, MNRAS, 334, 87
Woudt, P. A., Warner, B., & Motsoaledi, M. 2013, The Astronomer's Telegram, 4726, 1